ELSEVIER

Seismic and magnetic anisotropy of serpentinized ophiolite: Implications for oceanic spreading rate dependent anisotropy

D.R. Schmitt [a,*], Z. Han [a,1,2], V.A. Kravchinsky [a,2], J. Escartin [b]

[a] Inst. for Geophysical Research, Department of Physics, University of Alberta, Edmonton, Alberta, Canada T6G 2J1
[b] Inst. du Physique du Globe, Geosciences Marines, Case 89 IPGP- 4 P. Jussieu, 75252, Paris- Cedex 05, France

Abstract

Compressional and shear wave anisotropy, shear wave birefringence, and the anisotropy of magnetic susceptibility were measured on a series of dunites sampled from the Dinardic–Hellenic ophiolites. The densities of these materials ranged from 3330 kg/m^3 to 2620 kg/m^3 and indicate degrees of serpentinization from 2.3% to 87.9%, respectively.

Magnetic susceptibility increases and the compressional and shear wave velocities decrease in proportion to the degree of serpentinization as has been observed by other workers. In all cases the magnetic susceptibility tensor is described by an oblate spheroid whose minor axis is closely aligned to the pole of the foliation, but the magnetic anisotropy is not related to the degree of serpentinization. The compressional wave anisotropy ε monotonically decays from 12% for nearly pure olivine dunite to less than 2% for the most serpentinized sample; this observation strongly suggests that serpentinization progressively destroys the original anisotropy by consuming the preferentially aligned olivines and replacing them with randomly oriented serpentines. Typical serpentine mesh textures seen in microscopic thin section examinations support this suggestion. This loss of anisotropy with serpentinization may partly explain the apparent relationship between seismic compressional wave anisotropy of the oceanic lithosphere. The more complex geological structure of slow spreading ridges may admit more sea water via faults for deep circulation which increases serpentinization and consequence of which is decreased seismic anisotropy.
© 2007 Elsevier B.V. All rights reserved.

Keywords: seismic anisotropy; magnetic susceptibility; serpentine; dunite; ophiolite; ridge spreading

1. Introduction

Geological observations have shown that partially serpentinized peridotites may be an important compo-nent of the oceanic lithosphere particularly that formed at slow spreading ridges (Cannat, 1993) Serpentine is important for two reasons as, first, it strongly influences physical properties and consequent geophysical inter-pretations and, second, it is a major carrier of water into the mantle via subduction (Carlson and Miller, 2003; Bolfan-Casanova, 2005). Formation of the classic ophiolite based 'Penrose 1978 Model' compositionally layered oceanic lithosphere (Dilek, 2003) with a magmatic crust (Layers 2 and 3) overlying the mantle (Layer 4) may be restricted to fast-spreading ridges. The

* Corresponding author. Tel.: +1 780 492 3985; fax: +1 780 492 0714.
  E-mail address: schmitt@phys.ualberta.ca (D.R. Schmitt).
[1] Now at Shell Canada Resources, P.O. Box 100 Station M, Calgary, Alberta, Canada T2P 2H5.
[2] Tel.: +1 780 492 3985; fax: +1 780 492 0714.

structures at slow-spreading ridges are more heterogeneous, with gabbro intruding into mantle peridotite with varying degrees of alteration (Cannat, 1993, 1996). Recent reflection profiles obtained on the flanks of the intermediate-spreading Juan de Fuca ridge flank (Neimovic et al., 2005) may support this hypothesis.

Serpentinization, which results from the hydration of ultramafic minerals by seawater penetration (Aumento and Loubat, 1971), significantly influences the elastic and magnetic physical properties of the altered rocks. Anisotropy, or the lack thereof, in these attributes may be part of the key to resolving issues related to the interpretation of geophysical observations in two ways.

First, magnetite is a by-product of the release of Fe during serpentinization of olivine and pyroxene. Extensive studies on serpentinized cores from ODP drilling (Bina and Henry, 1990; Toft et al., 1990; Oufi et al., 2002) indicated that the magnetic susceptibility K depends inversely and logarithmically on the extent of serpentinization. The implications of anisotropy of the magnetic susceptibility on geophysical observations have not, to our knowledge, been extensively explored. However, the above laboratory studies, and that of Lawrence et al. (2002) on similar rock but with a different provenance, generally indicate that the magnetic susceptibility tensor is described by an oblate spheroid with the weakest component K_{min} perpendicular to the foliation.

Chemical remnant magnetization (CRM) via serpentinization of the lower crust and uppermost mantle is consistent with a number of observations. Arkani-Hamed and Strangway (1986) needed to invoke a thick (~35 km) and moderately magnetized ($K=0.0085$ SI) layer to explain the long-wavelength components of the oceanic magnetic field detected at high altitudes with MAGSAT. Similarly, high-frequency components of sea-level magnetic field in the vicinity of slow-spreading ridges require a two level geological lithosphere (Dyment et al., 1997; Gac et al., 2006). This structure broadly consists of an upper thermally remnant magnetization (TRM) layer formed soon after emplacement underlain by a second layer subject temporally dependent magnetite CRM upon cooling, circulation of water, and serpentinization.

Second, the average seismic velocities of peridotite monotonically decrease with the extent of serpentinization from about ~8 km/s to ~5 km/s and ~5 km/s to ~2 km/s for compressional and shear waves, respectively, as recently reviewed by Christensen (2004). This trend is evident in the compilation of earlier laboratory measurements of V_P and V_S (Fig. 1a) versus density, or equivalently in altered peridotites, serpentine content.
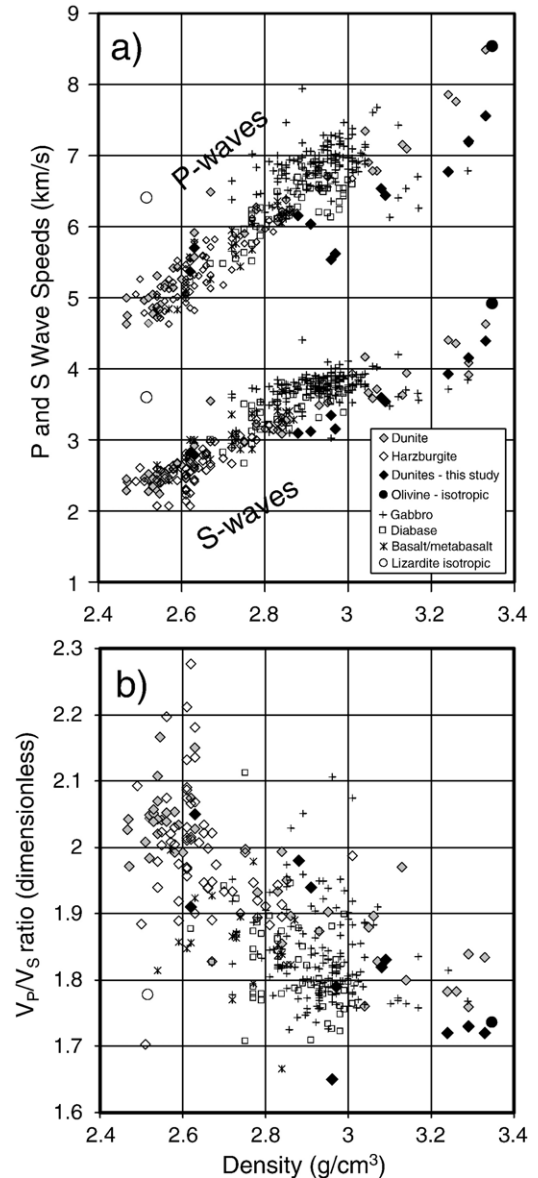

Fig. 1. a) Compressional and shear wave velocities measured at or near 100 MPa confining pressure of serpentinized dunites, harzburgites, gabbros, and basalts/metabasalts and diabases versus density. Values compiled from references (Christensen, 1966; Christensen, 1972; Christensen, 1978; Iturrino et al., 1991; Miller and Christensen, 1994; Iturrino et al., 1995; Horen et al., 1996; Itturino, 1996; Johnston and Christensen, 1997) including averaged values from this study plotted later in more detail. Isotropic values calculated from single crystal elastic constants for San Carlos olivine (Webb, 1989) and lizardite (Auzende et al., 2006). b) Compressional wave to shear wave velocity ratio versus density of the values from a). Symbols have the same meaning as in a).

Examination of Fig. 1 illustrates that it is impossible to unequivocally discriminate, on the basis of seismic velocities alone, a partially (10% to 40%) serpentinized

upper mantle peridotite from a intrusive gabbro both whose velocities lie between 6.1 km/s and 7.5 km/s (Horen et al., 1996; Carlson, 1998). Other physical characteristics that could distinguish gabbro and diabase from serpentinized peridotite must be employed. Carlson and Miller (1997) suggested that the lower shear wave velocities of serpentinized peridotites relative to gabbro/diabase (Figs. 1b and 2) provided one discriminating characteristic. Note that in these Figs. 1 and 2 the values for isotropic monocrystalline aggregates of both San Carlos olivine (Cholach, 2004) (Fo$_{0.9}$Fa$_{0.1}$) based on the elastic moduli measurements of Webb (1989) and recent *ab initio* calculations (Auzende et al., 2006) for lizardite are included for comparison. As such, field measurements of the V_P/V_S ratio (Fig. 1b) could indicate the proportion of serpentine in the lower oceanic crust.

Seismic anisotropy has also been put forward as a possible indicator of serpentinization (Dewandel et al., 2003). Elastic anisotropy suggests preferential alignment of olivine during extension of the lithosphere in the spreading direction, a contention supported by statistical studies of crystal orientations in ophiolites (Salisbury and Christensen, 1978; Christensen and Smewing, 1981). Generally, the compressional wave seismic anisotropy of upper mantle (Layer 4) is consistent with the shear-induced peridotite textures anticipated by plate spreading models. Although there are only a limited number of deep refraction studies in which azimuthal anisotropy of Layer 4 has been determined, various workers beginning with Hess (1964) observed that the direction of fast compressional wave velocities V_P for

Layer 4 coincide with that of sea-floor spreading. The degree of compressional wave anisotropy appears to depend on spreading rate with 3% to 4% seen in the slow-spreading North Atlantic (Keen and Tramonti, 1970; Gaherty et al., 2004), ∼5.5% in the in old Pacific lithosphere presumably produced at a fast-spreading ridge (Shearer and Orcutt, 1986), ∼7% near the fast-spreading East Pacific Rise (Dunn et al., 2000), and up to 10% of the intermediate-spreading Juan de Fuca ridge (Keen and Barrett, 1971; Au and Clowes, 1984). In contrast, in the few studies in which shear waves have been measured the corresponding Layer 4 shear wave velocities V_S do not appear to be anisotropic (Clowes and Au, 1982; Au and Clowes, 1984; Shearer and Orcutt, 1986).

While there are many measurements of the bulk magnetic susceptibility k and elastic wave velocities properties of serpentinized rocks, the anisotropy of these materials has not been much studied and never, to our knowledge, have both characteristics been obtained on serpentinized peridotites. Such comparisons have recently given valuable insights into pore structure and permeability (e.g. Benson et al., 2005). Here, the magnetic and elastic anisotropies of a series of ophiolitic dunites subject to varying degrees of serpentinization are determined. The bulk values and V_P anisotropy of both properties are found to depend on the serpentine mode. Although this is an exploratory study, the results may have implications that shed light on some of the observed differences in the geophysical responses of fast-versus slow-spreading ridges. A second, and practical implication, may be that the simpler AMS measurements may be useful in orienting material for more complex elastic wave measurements in lieu of more definitive descriptions of material texture.

2. Samples and preparation

Dunites with varying degrees of serpentinization were sampled from the Pindos and Vourinos ophiolites of Greece (Ross and Zimmerman, 1996). These Dinardic–Hellenic ophiolites were obducted during various closure pulses of the Tethyan Seas. Hand samples were examined visually to determine the foliation ($X–Y$ plane) and lineation (X-axis) (Fig. 3). As many cylindrical core plugs (2.54 cm diameter) were cut from each hand sample as possible, but in most cases only Y and Z (foliation perpendicular direction) directed cylinders were obtained and in three cases only Z-parallel samples could be cored.

Details of the material characterizations are given in Han (2005) and are only briefly presented here. Grain
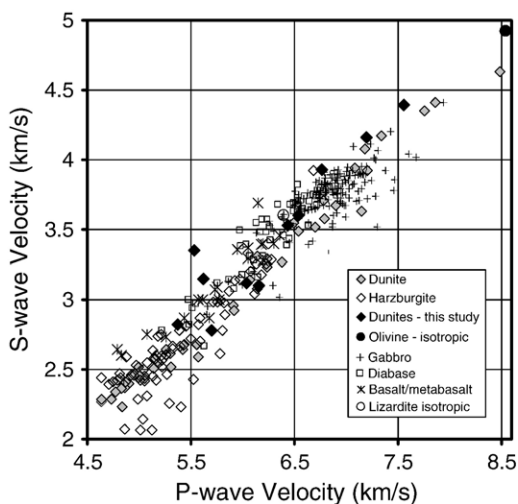

Fig. 2. Averaged shear wave velocities versus compressional wave velocities of materials from Fig. 1, symbols have same meaning as in Fig. 1.
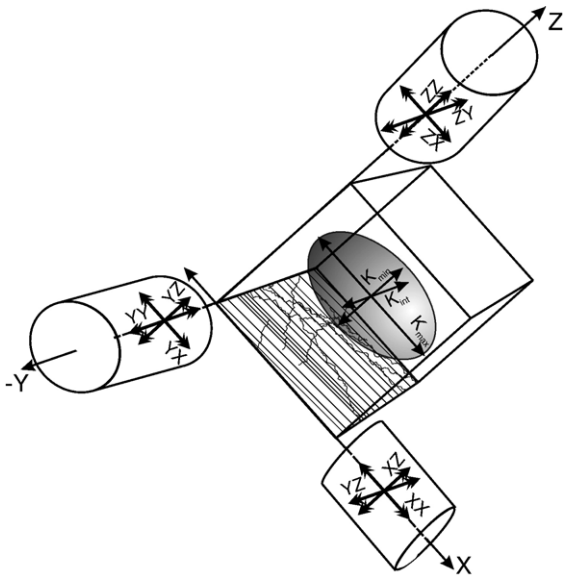
Fig. 3. Geometry of elastic wave and magnetic measurements in the textural element X–Y–Z co-ordinate frame. The lineation direction X lies within the X–Y foliation plane. The X–Y–Z axes are presumed to coincide with the principle axes for a material of orthorhombic symmetry. The three-dimensional elliptical surface describes the magnetic susceptibility tensor with principle axes K_{max}, K_{int}, and K_{min} shown coinciding with the X–Y–Z co-ordinates.

densities ρ_g as determined using a He-pyncnometer ranged from 2620 kg/m^3 to 3330 kg/m^3 which together with the corresponding bulk densities ρ_b ranging from 2600 kg/m^3 to 3280 kg/m^3 suggested porosities that range from negligible to nearly 0.024. This low, or even vanishing, porosity is consistent with SEM images that show no porosity, with the small pressure dependence of the P- and S-wave speeds as shown later, and with permeabilities below detection level. Using Miller and Christensen's (Miller and Christensen, 1994) relationships these densities yield a degree of serpentinization ranging from 2.3% to 87.9%. While density is often used as proxy for the degree of serpentinization, we have preferred retaining the density as the parameter against which the seismic and magnetic parameters are plotted in this paper. Other workers have used measures of the amount of magnetite to indicate serpentine content (Bina and Henry, 1990).

Three orthogonal thin sections, aligned with the metamorphic textural elements, were cut from each sample for analyses. Cyclic extinction of the olivines during rotation of the thin section under cross-polarizers indicates a preferential crystallographic olivine alignment that is not present in the serpentine portions. The textures of the three thin sections in Fig. 4 differ significantly. The high density and weakly serpentinized

sample is primarily composed of millimetre scale olivine crystals with numerous crosscutting serpentine-filled cracks. In contrast, the low density, highly serpentinized sample has a chaotic appearance with few remaining clear
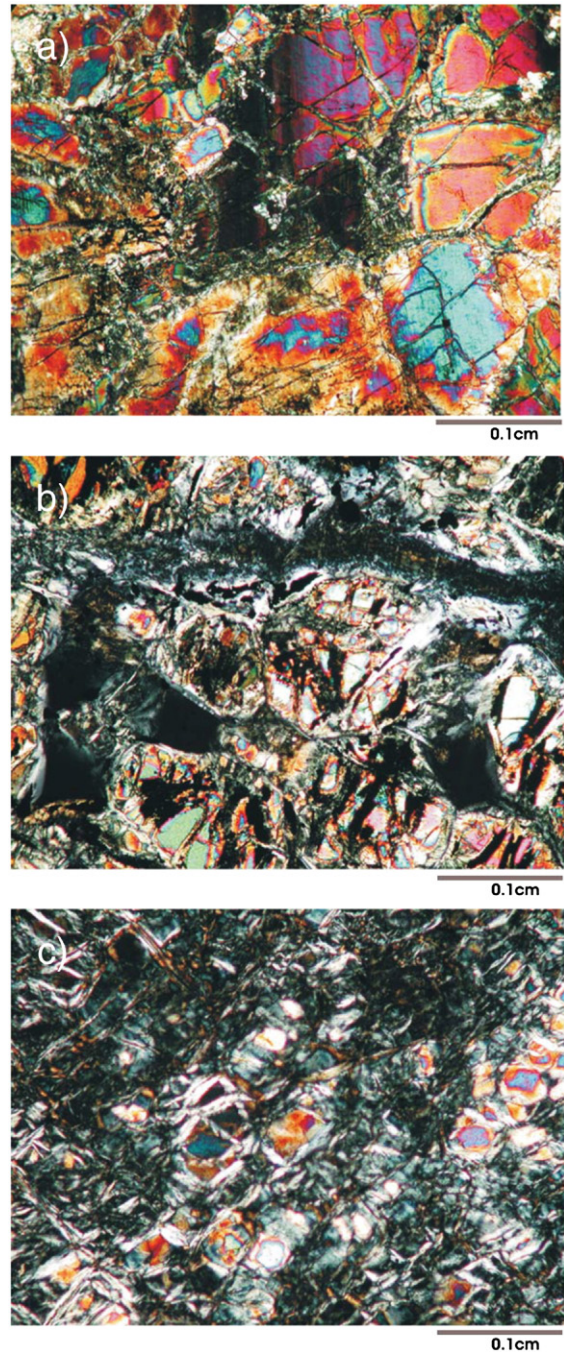

Fig. 4. Thin section photographs of a high density, largely unaltered dunite (Sample P03-1), a moderately altered dunite (Sample P16-3) and a low density, highly serpentinized dunite (Sample P13-1). Images taken at 50× magnification under cross-polarization.

crystals of olivine. The darker portions of the image are predominantly serpentine that appears in what has been referred to as 'apparent' fabrics by O'Hanley (1996).

Powder X-ray diffractometry found forsterite, clinochrysotile and lizardite serpentines, and detected enstatite and brucite in some of the samples. It is important to note that no antigorite serpentine was detected in these analyses. Antigorite is the high temperature polymorph; its lack of presence indicates that these samples should be considered as low temperature lizardite–chrysotile serpentinites (e.g., Evans, 2004). The antigorite in high temperature sepentinites appears to be more preferentially oriented and hence causes seismic wave anisotropy (Kern and Tubia, 1993; Watanabe et al., 2007); care need be exercised when interpreting the present results to higher temperature regions such as, for example, the mantle wedge above a subducting oceanic plate.

The complexity and heterogeneous nature of these textures (e.g. Fig. 4c) precluded point counting modal analysis. Alternatively, quantitative inversion of the conventional XRF whole rock oxide determinations using grain densities indicated the rocks were primarily composed of olivine ($Fo_{0.9}Fa_{0.1}$) and serpentine family minerals. It is interesting to note that the loss of volatiles during preparation for the whole rock analysis (loss on ignition LOI) is highly linearly dependent on the ρ_g further suggesting that the density of the material is a good indicator of the degree of serpentinization (Table 1).

3. Measurement techniques

One P-wave and two orthogonal S-wave velocities were measured at hydrostatic confining pressures of up to 300 MPa in steps of 25 MPa and at room temperature on each cylindrical sample plug using 1-MHz laboratory prepared transducers as described by Cholach et al. (2005). Standard pulse transmission methods were employed with transducers placed at both ends of the sample and with the transit time assumed to be given by the first extremum of the observed waveform. An example of a suite of shear wave forms obtained during a pressurization cycle to 300 MPa and back on one sample is shown in Fig. 5a. The polarizations of the shear wave transducers were individually oriented with the textural elements (X–Y–Z) of the material in order to obtain distinct mode arrivals. Wave speeds given are the simple ratio between sample length and transit time. Our estimate of the wave speed uncertainty is ∼1%, owing to the small changes in length of the sample that we have not accounted for (<0.3% at 300 MPa), and to the time picking errors. It is important to note that the velocities
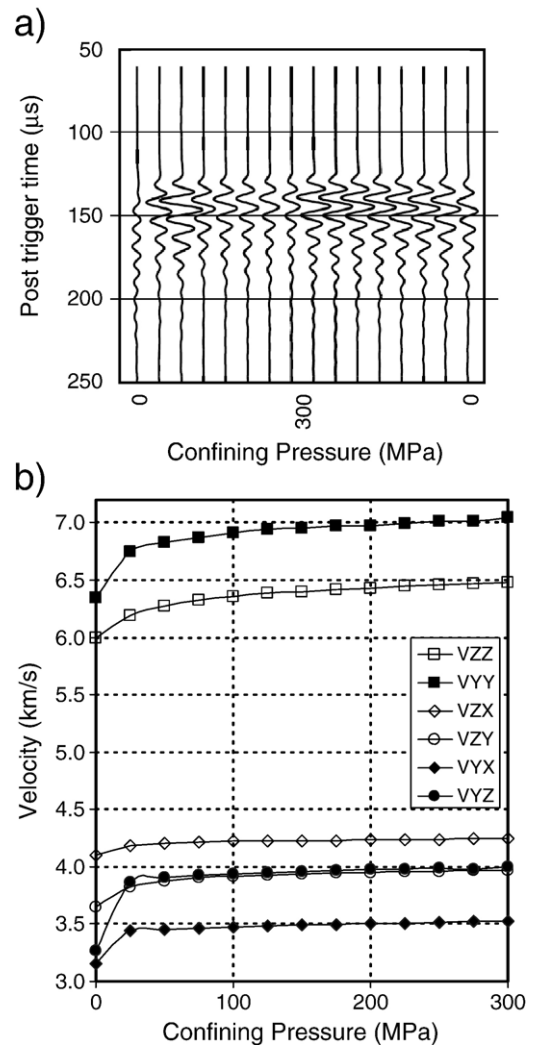

Fig. 5. a) Typical set of waveforms for shear waves acquired during pressurization from room pressure to 300 MPa and back for sample P11-1. b) Observed velocities versus hydrostatic confining pressure during the initial pressurization to 300 MPa on an Z-and a Y-oriented core plugs from relatively unaltered dunite sample P03-1 (density=3.19 g/cm^3). See text and Fig. 2 for the description of the various P-wave (V_{ZZ} and V_{YY}) and S-wave (V_{ZX}, V_{ZX}, V_{YX}, V_{YZ}).

in all the samples changed little with confining pressure (Fig. 5b), this is further indicative of low amounts of micro-crack porosity in agreement with the small porosities measured.

The velocity of a given wave mode will depend on both the directions of wave propagation and of particle polarization; these are denoted by the first and second subscripts, respectively, below. For example, V_{XX} refers to the compressional P-wave propagating parallel to the X-axis, and V_{ZY} indicates the shear wave propagating in the Z-direction with a transverse Y-direction polarization

(Fig. 3). A number of differing elastic wave anisotropies are defined based on the correspondence of polarizations within the textural planes of both the compressional and the various shear waves under the assumption the material has orthorhombic symmetry the principle axes of which align with the selected textural X–Y–Z co-ordinate system as described in Fig. 3. The following parameters:

1. P-wave (after Thomsen, 1986): $\varepsilon = (V_{ZZ} - V_{YY})/V_{ZZ}$,
2. SH mode in Z–Y plane (Thomsen, 1986): $\gamma = (V_{YX} - V_{ZX})/V_{ZX}$,
3. SV mode in Z–Y plane: $\chi = (V_{YZ} - V_{ZY})/V_{ZY}$,
4. S-wave splitting along the Z axis: $\Delta ZV_S = (V_{ZY} - V_{ZX})/V_{ZX}$,
5. S-wave splitting along the Y axis: $\Delta YV_S = (V_{YZ} - V_{YX})/V_{YX}$ are defined in order to better characterize the anisotropy of the material. In the three planes of symmetry of an orthorhombic medium, the 'qP' and 'qSH'-mode anisotropies mimic those for transversely isotropic (TI) media (Tsvankin, 1997) while χ, ΔZV_S, and ΔYV_S are introduced here to deal with the added complexities of orthorhombic anisotropies to the degree that this is possible with the measurements made. Following Thomsen (1986), these measures of anisotropy are directly related to the symmetry based material elasticity.

More traditionally, however, a variety of calculations have been used to report quantitative values of anisotropy throughout the literature. For example, Birch (1960) calculated the P-wave anisotropy AV_P as the ratio of the difference of the observed maximum and minimum velocities to the arithmetical average. Similarly, reported S-wave anisotropies are calculated using averages but this is further complicated by shear wave splitting. Consequently, Kern and Tubia (1993) defined the S-wave anisotropy $AV_S = (V_{Smax} - V_{Smin})/V_S$ where V_S is the arithmetical mean of the measured shear wave velocities and V_{Smax} and V_{Smin} are the maximum and minimum values of the average of the two shear modes in a given direction. To facilitate comparison with earlier results these alternate measures of anisotropy are also included in the figures.

In order to better illustrate the complex shear wave behaviour of an orthorhombic material, the modelled shear wave velocities as a function of direction within the principle textural/orthorhombic planes for a strongly textured 'Type-I' dunite are presented in Fig. 6. It is important to note the various equalities of some of the shear wave velocities as for example: $V_{YZ} = V_{ZY}$ such that $\chi = 0$ for a perfect orthorhombic material. Cases in
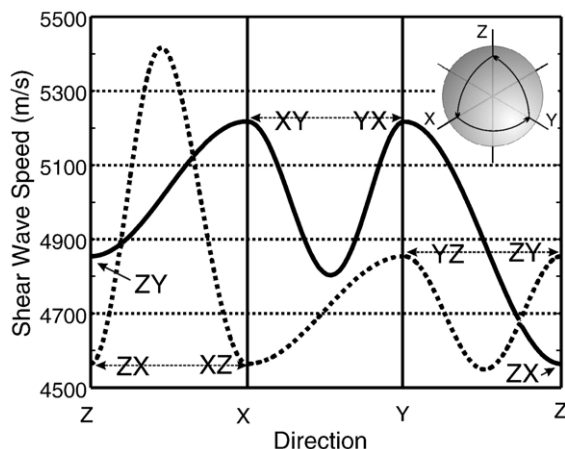

Fig. 6. Illustrative example of the variations of the two shear wave speeds with direction along the path beginning at $Z \rightarrow X \rightarrow Y \rightarrow Z$ in a textured dunite with orthorhombic symmetry. Phase velocities are calculated using a geometric-mean approach by Cholach (2004) for a 'Type-I' texture with the peaks of the probability distribution orientations of the olivine [100], [010], and [001] crystal axes parallel to the X, Z, and Y axes, respectively. The phase velocity calculations employ the elastic stiffnesses $C_{11} = 289.6$ GPa, $C_{22} = 221.8$ GPa, $C_{33} = 200.5$ GPa, $C_{44} = 75.9$ GPa, $C_{55} = 67.1$ GPa, $C_{66} = 87.7$ GPa, $C_{12} = 103.9$ GPa, $C_{13} = 49.3$ GPa, and $C_{23} = 77.4$ GPa with a density $\rho = 3221$ kg/m^3.

which $\chi \neq 0$ could indicate misalignment of the samples from the principal planes, anisotropies that deviate from orthorhombic symmetry, or heterogeneity within the sample. It is interesting to note that the observed set of 6 velocities of Fig. 5b are suggestive of orthorhombic symmetry for that sample, most notably as $V_{ZY} = V_{YZ}$.

Magnetic anisotropy (or Anisotropy of Magnetic Susceptibility — AMS) was measured on the same cylindrical core plugs but after shortening to 2.54 cm length. The magnetic susceptibility ellipsoid described by the orientations and three principle values K_{max}, K_{int}, and K_{min} of the 2nd order susceptibility tensor were determined using an 18-position system, (Barrington MS2B sensor, with AMSWIN-BAR software). The mean magnetic susceptibility is here given as $K = (K_{max} + K_{int} + K_{min})/3$ and the magnetic anisotropy is $\kappa = (K_{max} - K_{min})/K$. The magnetic susceptibility tensor as represented as an ellipsoid in Fig. 2, may also be described with the parameters of the corrected anisotropy P_J defined by Jelinek (1981)

$$P_J = \exp \sqrt{\{2[(\eta_1 - \eta_m)^2 + (\eta_2 - \eta_m)^2 + (\eta_3 - \eta_m)^2]\}}$$

where $\eta_i = \ln K_i$ ($i = 1$, 2, or 3) and $\eta_m = (\eta_{max} + \eta_{int} + \eta_{min})/3$. The shape of the anisotropy ellipsoid can be expressed in terms of the ratios or differences of the axial

values. Most early parameters were based on ratios as for example the lineation of Balsey and Buddington (1960): $P_1 = L = K_{max}/K_{int}$ and the foliation of Stacey (1960):

a)

$P_3 = F = K_{int}/K_{min}$ but more recent descriptions employ the shape parameter T

$$T = \frac{2\ln(K_{int}/K_{min})}{\ln(K_{max}/K_{min})} - 1$$

which indicates whether the ellipsoid is prolate ($T<0$) or oblate ($T>0$). These values are provided in the electronic supplementary material.

4. Results and discussion

4.1. Magnetic anisotropy

The magnetic properties display two relationships. First, the orientations of the magnetic principle axes (Fig. 7a) show a clear clustering of K_{min} orientations parallel to Z with K_{max} and K_{int} trending to lie close to the X–Y foliation plane. These results are consistent with the recent AMS observations of Lawrence et al. (2002) despite the differing provenance of their serpentinized peridotites. This suggests that magnetic AMS measurements may be able to provide an early indication of the sample metamorphic texture that could direct later preparations for more complex elastic wave measurements. Second, as noted earlier, k is roughly inversely dependent on density (Fig. 7b) owing to the formation of magnetite as a by product of the release of Fe during serpentinization of olivine and pyroxene (see also Aumento and Loubat, 1971; Bina and Henry, 1990). Finally, all the samples all are magnetically anisotropic with an oblate shape of the magnetic tensors (Fig. 7c). However, the degree of anisotropy κ is not related to the extent of serpentinization or density (Fig. 8).

Although, the shape of the AMS ellipsoid is determined by both ferromagnetic and paramagnetic grain and crystal orientations, the accessory minerals such as magnetite usually have susceptibilities that are three orders of magnitude larger than those of the original paramagnetic matrix-forming olivines and pyroxenes. However, ferromagnetic magnetite, a typical chemical product of serpentinization, has by itself a low AMS value with an ellipsoid that is nearly spherical;
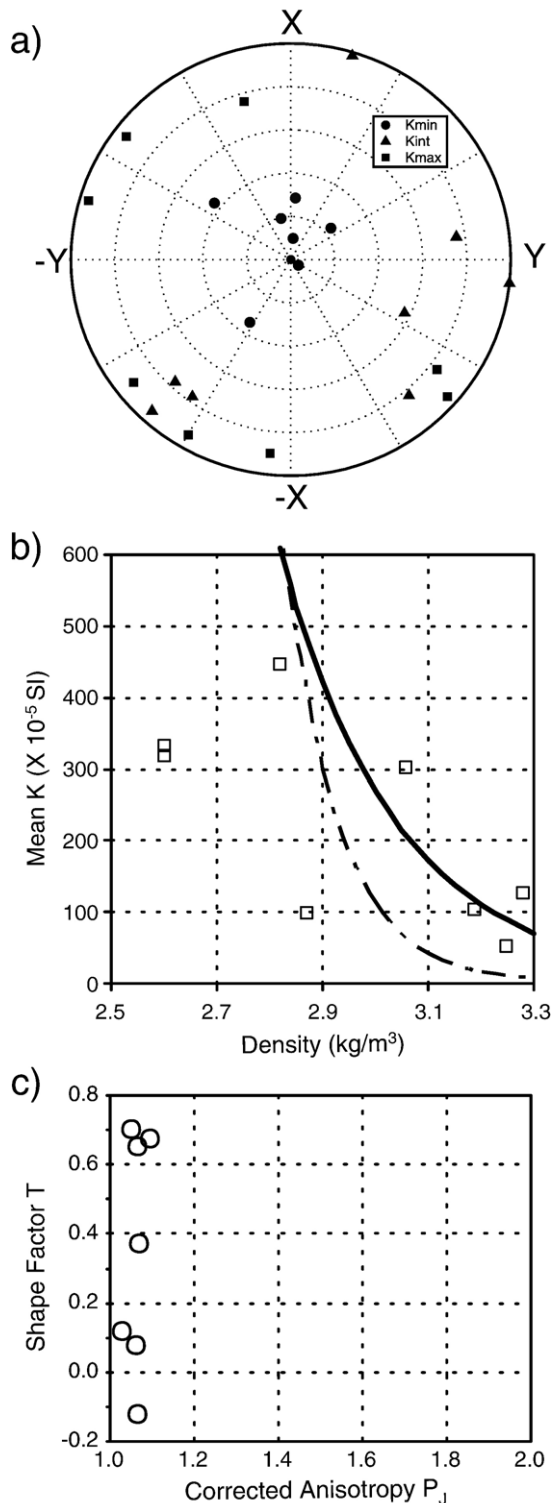
Fig. 7. Magnetic characteristics of the samples. a) Equal area projection of principle magnetic components as relative to the rock textural elements. The vertical pole of the figure is perpendicular to the foliation plane as seen in hand sample. b) Mean magnetic susceptibility versus density (open squares). Best fit lines from Toft et al. (1990) (heavy continuous line) and Oufi et al. (2002) (light broken line) are shown for comparison. c) Magnetic corrected anisotropy P_J versus magnetic shape parameter T.
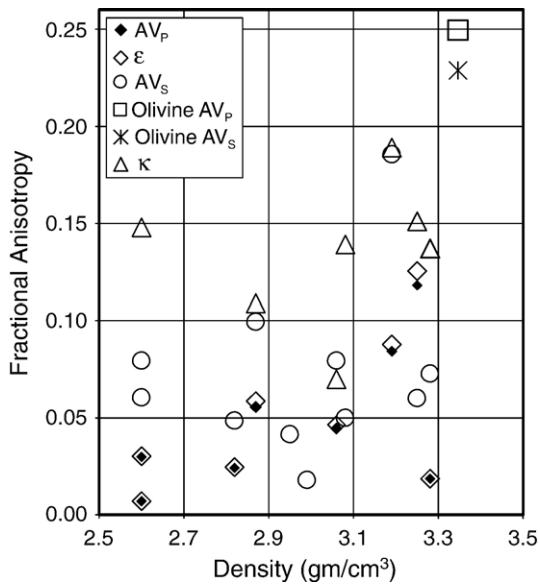
Fig. 8. Fractional anisotropy for the magnetic κ, P-wave AV_P and ε, and S-wave AV_S versus density. Olivine values are those calculated from single crystal elastic moduli given by Webb (1989).

greater proportions of magnetite are thus expected to reduce the magnetic anisotropy initially produced by the paramagnetic mineral assemblage. Values of the parameter P_j (Fig. 7c and Tables in supplementary material) are low (from 1.031 to 1.095) and suggest that the AMS of our samples is mostly controlled by magnetite. Thermomagnetic experiments also revealed a Curie temperature of 580 °C which is highly suggestive of the presence of magnetite. The observed magnetic anisotropy κ varies from 7.0% to 18.9% (Fig. 8) and this may suggest the presence of some paramagnetic anisotropy. However a correlation between degree of serpentinization (higher degree presumes larger production of magnetite) and the AMS was not observed in the samples. The paramagnetic component could likely be responsible for a change of the AMS ellipsoid toward the disk-shaped parameter T_j.

4.2. Elastic wave anisotropy

All the elastic wave velocities decrease with serpentine content (Fig. 9) in agreement with earlier experimental measurements recently summarized by Christensen (2004) (Fig. 1a). The P-wave anisotropy ε also decreases with density from a high of 12% to nearly zero (Fig. 8), note that the traditional AV_P and symmetry based ε P-wave anisotropy measures are close to one another.

The decline of ε is of interest as there are only a few measurements of anisotropy made on such materials.

Kern and Tubia (1993) measured P- and S-wave anisotropy on cubes of serpentinized ultramafic rocks from the Sierra Alpujata massive, Spain. Their measurements to 600 MPa and 600 °C, which were conducted in three cubical samples oriented with respect to the rock lineation and foliation, showed that the P-wave anisotropy declined from 6–8% in a fresh lherzolite to less than 2% in the more altered sample. Similarly, Horen et al. (1996) measured P and S wave velocities at room pressure on six serpentinized peridotites from the Xigaze ophiolite with density estimated degrees of serpentinization from 3% to 70%. They too report a decrease in the P-wave anisotropy and also in the S-wave anisotropy. A direct comparison with our results is complicated as these studies do not report how anisotropies are determined with respect to the textural elements, nor what shear wave polarizations were measured and used in their
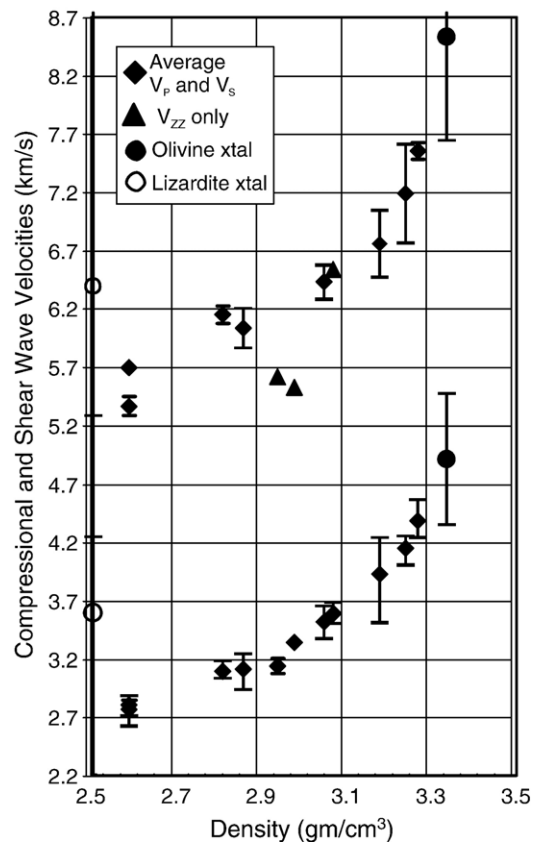

Fig. 9. Compressional and shear wave velocities versus density. Symbols represent the average of the observed velocities for a given sample and the error bars indicate the maximum and minimum observed velocities. The average values for olivine and lizardite are those calculated for an isotropic aggregates by Cholach (2004) and Auzende et al. (2006), respectively, with the error bars representing the extremum velocities for the single crystals.

calculations. Further, as pressure was not applied to their samples it is also difficult to know how cracks may influence the velocity and particularly the anisotropy.

In contrast, Dewandel et al. (2003) came to a differing conclusion in a modelling study of an Oman ophiolite. They found a strongly textured lizardite filling an interpenetrative vein network in one of their samples. They modelled the elastic properties of the rock assuming that strongly oriented ellipsoidal inclusions of serpentine (using chlorite elastic properties as an analog) lay within a harzburgite with preferentially oriented olivine and enstatite. This arrangement increased the anisotropy of the original textured harzburgite by a few percent; and on this basis they suggested that increased anisotropy might allow for discrimination of serpentinized peridotites from gabbros at the base of Layer 3.

Most recently, Song et al. (2004) made P and S wave measurements both perpendicular and parallel to the strong foliation plane on three serpentinites taken from a quarry. The densities of these materials are low (2.640 g/cm^3 to 2.740 g/cm^3) and may suggest they are nearly completely serpentinized although there is no petrologic description given. In contrast to the current observations, they saw relatively high P wave anisotropy for all three of their samples of nearly 9%. The reason for this discrepancy is not known, it may be related to the deformation their material has undergone. Further, their samples have a clear 'layered' appearance both in macroscopic hand sample and under thin section, and it is this layering that could be contributing to their observed anisotropy also.

In the current study, ε was measured in seven dunites spanning a range of degrees of serpentinization and the anisotropy decreases nearly monotonically from over 12% to less than 1% (Fig. 8) The cyclic optical extinction of the olivines in all the samples suggests that they were preferentially aligned prior to alteration and hence originally elastically anisotropic. It is important to note that serpentine minerals and their placement with in rocks is complex. Serpentinization preferentially initiates around grain boundaries and evolve to form a 'mesh texture' (Wicks and Whittaker, 1975, 1977; Maltman, 1978) increasing aletion in addition to the pre-existing veins cross-cutting the rock. Serpentinite (lizardite) grains formed during static serpentinization tend to grow perpendicular to the original grain boundaries, resulting in an overall complex and random texture with no overall lattice preferred orientation (e.g. Fig. 2b). O'Hanley (1996) discusses details of the complex textures observed in serpentinized peridotites. He notes the difficulties in identifying these minerals and noting that 'microbeam X-ray' techniques may be necessary to

study the small serpentine mineral grains. Taken together it appears that in these samples the serpentine crystals are not preferentially aligned and hence will decrease the original anisotropy unaltered protolith in proportion to the extent of serpentinization.

In contrast, there appears to be no systematic relationship between the shear wave anisotropy AV_S (Fig. 8) or shear wave splitting ΔZV_S and ΔYV_S (Fig. 10) and the serpentine content. Most of the AV_S values fall within the range of 5% to 10%. Similarly, shear wave splitting in both directions mostly range ± 7% with no apparent trend with density. These observations suggest that substantial shear wave anisotropy remains even with highly serpentinized material, which otherwise appears nearly isotropic to P-waves.

The reason for this contradictory behaviour is not yet clear. One possible reason may be heterogeneity, although for a given sample this is not expected to be a serious issue as the grain density of the cores cut from a given sample rarely differed by more than 1%. Another possible reason could be the accumulation of errors in properly orienting the samples with respect to the textural X–Y–Z elements particularly during coring. A Examination of the illustration of Fig. 6 shows that the shear wave birefringence can be particulary sensitive to small deviations from the principal directions; slight deviations could result in larger shear wave splitting than anticipated. A final reason may be that the samples may be less
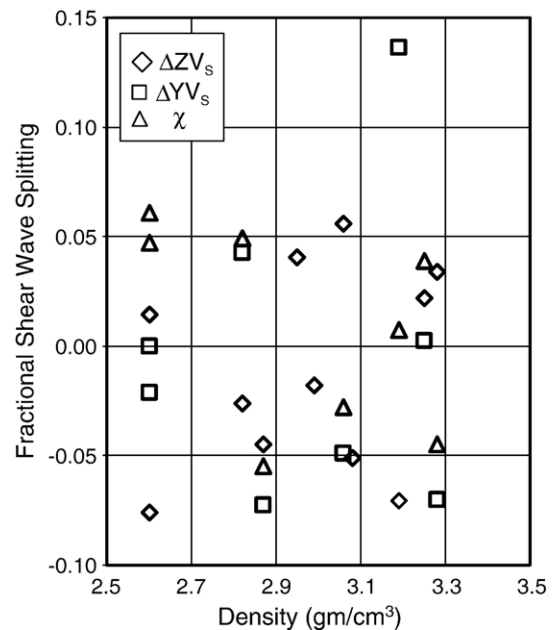

Fig. 10. Fractional shear wave splitting ΔZV_S and ΔYV_S and SV-mode fractional difference χ versus density.

symmetric than the orthorhombicity assumed here, and this would lead to more complex shear wave splitting. At present, this remains unresolved.

4.3. Implications

The oceanic mantle anisotropy is presumed to result from the magmatic fabric acquired during shearing of the material in the plastic regime. Consequently, one is tempted to simply ascribe the inverse relationships between compressional wave anisotropy and spreading rate to increased serpentinization in slower spreading ridges. This destruction of the initial olivine anisotropy by serpentinization, however, likely contributes strongly to the loss of seismic anisotropy but other factors, related to the geological structure, cannot be ignored. For example, in a slow-spreading ridge, once the mantle rocks pass the brittle–ductile transition and are accreted in the lithosphere, they are tectonically uplifted at the ridge axis until they are exposed at the seafloor. This 'tectonic 'elevator is not fully understood, but these displacements must be accommodated by a complex set of faults, that are probably cross cutting. It has been postulated that this results in important tectonic rotations (one of the results of ODP Leg 209). A problem with this is that the sizes of the fault blocks are not yet known although sea-floor surface topography would suggest they have dimensions on the order of 1 to 10 km. A collection of these blocks with differing orientations will likely influence the observed level of anisotropy also.

Finally, while likely not a necessarily a causative relationship, the principal directions of the susceptibility tensor in these samples generally indicate the principal textural $X–Y–Z$ orientations. This suggests that determination of the magnetic orientations, which are readily measured in a tensor form the eigenvectors of which give the principal directions, may be useful as a guide in aligning samples for high pressure ultrasonic measurements in lieu of more definitive tests X-ray or optical methods. One advantage of magnetic AMS measurements is that they are inexpensive and rapid; determination of orientations of the principle magnetic axes may provide a better estimation of the true metamorphic textures that would be used to direct sub-sampling for elastic wave measurements. This likely could only be accomplished using sophisticated methods to obtain statistical representations of the crystallographic orientations in analogy to a similar study of the paramagnetic response of fresh dunites by Ferre et al. (2005) While the magnetic and rock textural elements correlate, there unfortunately does not appear to be any further relationship between the elastic anisotropy and either the severity of the magnetic anisotropy nor the magnitude of the magnetic susceptibility. This discounts any potential applicability of magnetic properties in the bulk oceanic crust as a proxy for elastic anisotropy.

5. Conclusions

Both the magnetic and elastic wave anisotropy were studied on a suite of ophiolitic dunites subject to varying degrees of serpentinization. Mean magnetic susceptibility increases and the elastic wave velocities decrease with increased alteration as has been found in earlier studies. The principle magnetic tensor axes generally align with the visually identified metamorphic textural elements with K_{min} perpendicular to the visually identified foliation plane.

The compressional wave anisotropy ε decays with increased serpentinization. In contrast, neither shear wave birefringence nor anisotropy appears to be systematically related to the amount of serpentine in the samples. The loss of P-wave anisotropy upon serpentinization may have implications to the interpretation of deep oceanic refraction studies. As noted above, oceanic refraction tests show that the compressional wave anisotropy within the mantle Layer 4 is generally oriented with respect to the spreading direction and that degree of anisotropy depends on spreading rate. Lower spreading rates are also associated in various models with increased heterogeneity, fracturing, and percolation of seawater to depth resulting in increased serpentinization. As a result, the dependence of seismic anisotropy on spreading rate may be a consequence of the decay of anisotropy upon serpentinization. This alteration depends temporally on the rate of spreading, cooling, and water percolation and suggests that the anisotropy will likely decline both in depth and distance from the spreading ridge with time. Whether such changes in anisotropy could be detected given the relatively poor resolution allowed in refraction seismic surveys is not clear. Alternatively, the persistence of Layer 4 anisotropy in all seismic field observations argues against pervasive serpentinization of the oceanic lower crust and uppermost mantle.

Appendix A. Supplementary data

Supplementary data associated with this article can be found, in the online version, at doi:10.1016/j.epsl.2007. 07.024.

References

Arkani-Hamed, J., Strangway, D.W., 1986. Effective magnetic susceptibility of the oceanic upper mantle derived from Magsat data. Geophys. Res. Lett. 13, 999–1002.

Au, D., Clowes, R.M., 1984. Shear wave velocity structure of the oceanic lithosphere from ocean bottom seismometer studies. Geophys. J. R. Astron. Soc. 77, 105–123.

Aumento, F., Loubat, H., 1971. The mid-Atlantic ridge near 45° N. Serpentinized ultramafic intrusions. Can. J. Earth Sci. 8, 631–663.

Auzende, A.L., Pellenq, R.J.M., Devouard, B., Baronnet, A., Grauby, O., 2006. Atomistic calculations of structural and elastic properties of serpentine minerals: the case of lizardite. Phys. Chem. Miner. 33, 266–275.

Balsey, J.R., Buddington, F., 1960. Magnetic susceptibility anisotropy and fabric of some Adirondack granites and orthogneisses. Am. J. Sci. 258, 6–20.

Benson, P.M., Meredith, P.G., Platzman, E.S., White, R.E., 2005. Pore fabric shape anisotropy in porous sandstones and its relation to elastic wave velocity and permeability anisotropy under hydrostatic pressure. Int. J. Rock Mech. Min. Sci. 42, 890–899.

Bina, M.M., Henry, B., 1990. Magnetic properties, opaque mineralogy and magnetic anisotropies of serpentinized peridotites from ODP Hole 670A near the Mid-Atlantic Ridge. Phys. Earth Planet. Sci. 65, 88–103.

Birch, F., 1960. The velocity of compressional waves in rocks to 10-kilobars. 1. J. Geophys. Res. 65, 1083–1102.

Bolfan-Casanova, N., 2005. Water in the earth's mantle. Min. Mag. 69, 229–257.

Cannat, M., 1993. Emplacement of mantle rocks in the seafloor at mid-ocean ridges. J. Geophys. Res. 98, 4163–4172.

Cannat, M., 1996. How thick is the magmatic crust at slow spreading oceanic ridges? J. Geophys. Res. 101, 2847–2857.

Carlson, R.L., 1998. Seismic velocities in the uppermost oceanic crust: age dependence and the fate of layer 2a. J. Geophys. Res. 103, 7069–7077.

Carlson, R.L., Miller, D.J., 1997. A new assessment of the abundance of serpentinite in the oceanic crust. Geophys. Res. Lett. 24, 457–460.

Carlson, R.L., Miller, D.J., 2003. Mantle wedge water contents estimated from seismic velocities in partially serpentinized peridotites. Geophys. Res. Lett. 30, 1250. doi:10.1029/2002GL016600.

Cholach, P.Y., The elasticity of intrinsically anisotropic rocks, Ph.D. Thesis, Department of Physics, University of Alberta, University of Alberta, Edmonton, Alberta, pp. 167., (2004).

Cholach, P.Y., Molyneux, J.B., Schmitt, D.R., 2005. Flin Flon belt seismic anisotropy: elastic symmetry, heterogeneity, and shear wave splitting. Can. J. Earth Sci. 42, 533–544.

Christensen, N.I., 1966. Elasticity of ultrabasic rocks. J. Geophys. Res. 71, 5921–5931.

Christensen, N.I., 1972. The abundance of serpentinites in the oceanic crust. J. Geol. 80, 709–719.

Christensen, N.I., 1978. Ophiolites, seismic velocities and oceanic crustal structure. Tectonophysics 47, 131–157.

Christensen, N.I., 2004. Serpentinites, peridotites, and seismology. Int. Geol. Rev. 46, 795–816.

Christensen, N., Smewing, J.D., 1981. Geology and seismic structure of the northern section of the Oman Ophiolite. J. Geophys. Res. 86, 2545–2555.

Clowes, R.M., Au, D., 1982. In situ evidence for a low degree of S-wave anisotropy in the oceanic upper mantle. Geophys. Res. Lett. 9, 13–16.

Dewandel, B., Boudier, F., Kern, H., Warsi, W., Mainprice, D., 2003. Seismic wave velocity and anisotropy of serpentinized peridotite in the Oman ophiolite. Tectonophysics 370, 77–94.

Dilek, Y., 2003. Ophiolite pulses, mantle plumes and orogeny. In: Dilek, Y., Robinson, P. (Eds.), Ophiolites in Earth History. Geological Society, London, Special Publications, pp. 9–19.

Dunn, R.A., Toomey, D.R., Solomon, S.C., 2000. Three-dimensional seismic structure and physical properties of the crust and shallow mantle beneath the East Pacific Rise at 9 degrees 30'N. J. Geophys. Res. 105, 23537–23555.

Dyment, J., Arkani-Hamed, J., Ghods, A., 1997. Contribution of serpentinized ultramafics to marine magnetic anomalies at slow and intermediate spreading centres: Insights from the shape of the anomalies. Geophys. J. Int. 129, 691–701.

Evans, B.W., 2004. The serpentinite multisystem revisited: chrysotile is metastable. Int. Geol. Rev. 46, 479–506.

Ferre, E.C., Tikoff, B., Jackson, M., 2005. The magnetic anisotropy of mantle peridotites: example from the Twin Sisters dunite, Washington. Tectonophysics 398, 141–166.

Gac, S., Tisseau, C., Dyment, J., Jérôme, Goslin, J., 2006. Modelling the thermal evolution of slow-spreading ridge segments and their off-axis geophysical signature. Geophys. J. Int. 164, 341–358.

Gaherty, J.B., Lizarralde, D., Collins, J.A., Hirth, G., Kim, S., 2004. Mantle deformation during slow seafloor spreading constrained by observations of seismic anisotropy in the western Atlantic. Earth Planet. Sci. Lett. 228, 255–265.

Han, Z., Correlations between seismic and magnetic susceptibility anisotropy in serpentinized peridotite, M.Sc. thesis, Dept. of Physics, Univ. of Alberta, pp. 152 (2005).

Hess, H.H., 1964. Seismic anisotropy of the upper mantle under oceans. Nature 23, 629–631.

Horen, H., Zamora, M., Dubuisson, G., 1996. Seismic waves velocities and anisotropy in serpentinized peridotites from Xigaze ophiolite: abundance of serpentine in slow spreading ridge. Geophys. Res. Lett. 23, 9–12.

Itturino, G.J., A study of the nature of oceanic crustal reflectivity using laboratory and log measurements: based on results from the Deep Sea Drilling Project and Ocean Drilling Program site in the Pacific and Indian Oceans. Ph.D. thesis, University of Miami (1996).

Iturrino, G.J., Christensen, N.I., Kirby, S., Salisbury, M.H., 1991. Seismic velocities and elastic properties of oceanic gabbroic rocks from Hole 735 B. In: Von Herzen, R.P., Robinson, P.T. (Eds.), Proc. ODP, Sci. Results, vol. 118, pp. 227–244.

Iturrino, G.J., Christensen, N.I., Becker, K., Boldreel, L.O., Harvey, P.K.H., Pezard, P., 1995. Physical properties and elastic constants of upper crustal rocks from core-log measurements in Hole 504 B. In: Erzinger, J., Becker, K., Dick, H.J.B., Stokking, L.B. (Eds.), Proc. ODP, Sci. Results, vol. 137, pp. 273–291.

Jelinek, V., 1981. Characterization of the magnetic fabric of rocks. Tectonophysics 79, 63–67.

Johnston, J.E., Christensen, N.I., 1997. Seismic properties of layer 2 basalts. Geophys. J. Int. 128, 285–300.

Keen, C.E., Barrett, D.L., 1971. Measurement of seismic anisotropy in northeast Pacific. Can. J. Earth Sci. 8, 1056–1064.

Keen, C., Tramonti, C., 1970. A seismic refraction survey on mid-Atlantic ridge. Geophys. J. R. Astron. Soc. 20, 473–491.

Kern, H., Tubia, J.M., 1993. Pressure and temperature-dependence of P-wave and S-wave velocities, seismic anisotropy and density of sheared rocks from the Sierra Alpujata Massif (Ronda Peridotites, Southern Spain). Earth Planet. Sci. Lett. 119, 191–205.

Lawrence, R.M., Gee, J.S., Karson, J.A., 2002. Magnetic anisotropy of serpentinized peridotites from the MARK area: implications for the orientation of mesoscopic structures and major fault zones. J. Geophys. Res. 107 (No. 2073).

Maltman, A.J., 1978. Serpentine textures in Anglesey, North Wales, United Kingdom. Geol. Soc. Amer. Bull. 89, 972–980.

Miller, D.J., Christensen, N.I., 1994. Seismic signature and geochemistry of an island-arc — a multidisciplinary study of the Kohistan Accreted Terrane, Northern Pakistan. J. Geophys. Res 99, 11623–11642.

Neimovic, M.R., Carbotte, S.M., Harding, A.J., Detrick, R.S., Pablo Canales, J., Dieibold, J.B., Kent, G.M., Tischer, M., Babcock, J.M., 2005. Frozen magma lenses below the oceanic crust. Nature 436, 1149–1152.

Oufi, O., Cannat, M., Horen, H., 2002. Magnetic properties of variably serpentinized abyssal peridotites. J. Geophys. Res. 107, 19. doi:10.1029/2001JB000549.

O'Hanley, D.S., 1996. Serpentinites: Records of petrologic and tectonic history. Oxford Monographs in Geology and Geophysics, vol. 34. Oxford University.

Ross, J.V., Zimmerman, J., 1996. Comparison of evolution and tectonic significance of the Pindos and Vourinos ophiolite suites, northern Greece. Tectonophysics 256, 1–15.

Salisbury, M.H., Christensen, N.I., 1978. The seismic velocity structure of a traverse through the Bay of Islands Ophiolite Complex, Newfoundland, and exposure of oceanic crust and upper mantle. J. Geophys. Res. 83, 805–817.

Shearer, P.M., Orcutt, J.A., 1986. Compressional and shear wave anisotropy of the oceanic lithosphere the Ngendei seismic refraction experiment. Geophys. J. R. Astron. Soc. 87, 967–1003.

Song, I., Suh, M., Woo, Y.K., Hao, T.Y., 2004. Determination of the elastic modulus set of foliated rocks from ultrasonic velocity measurements. Eng. Geol. 72, 293–308.

Stacey, F.D., 1960. Magnetic anisotropy of igneous rocks. J. Geophys. Res. 65, 2429–2442.

Thomsen, L., 1986. Weak elastic anisotropy. Geophysics 51, 1954–1966.

Toft, P.B., Arkani-Hamed, J., Haggerty, S.E., 1990. The effects of serpentinization on density and magnetic susceptibility: a petrophysical model. Phys. Earth Planet. Inter. 65, 137–157.

Tsvankin, I., 1997. Anisotropic parameters and P-wave velocity for orthorhombic media. Geophysics 62, 1292–1309.

Watanabe, T., Kasami, H., Ohshima, S., 2007. Compressional and shear wave velocities of serpentinized peridotites up to 200 MPa. Earth Planets Space 59, 233–244.

Webb, S.L., 1989. The Elasticity of the Upper Mantle Orthosilicates Olivine and Garnet to 3 GPa. Phys. Chem. Miner. 16, 684–692.

Wicks, F.J., Whittaker, E.J.W., 1975. A reappraisal of the structures o the serpentinite minerals. Can. Miner. 13, 227–243.

Wicks, F.J., Whittaker, E.J.W., 1977. Serpentinite textures and serpentinization. Can. Miner. 15, 459–488.